Properties of photocurrent and metal contacts of highly resistive ultrawide bandgap semiconductors ⊘

A. Tingsuwatit (ID) ; N. K. Hossain (ID) ; Z. Alemoush (ID) ; M. Almohammad (ID) ; J. Li (ID) ; J. Y. Lin (ID) ;
H. X. Jiang ✉ (ID)

Check for updates

View Online   Export Citation

Properties of photocurrent and metal contacts of highly resistive ultrawide bandgap semiconductors

View Online   Export Citation   CrossMark

A. Tingsuwatit, [ID] N. K. Hossain, [ID] Z. Alemoush, [ID] M. Almohammad, [ID] J. Li, [ID] J. Y. Lin, [ID] and H. X. Jiang[a) [ID]

AFFILIATIONS

Department of Electrical and Computer Engineering, Texas Tech University, Lubbock, Texas 79409, USA

[a)]Author to whom correspondence should be addressed: hx.jiang@ttu.edu

ABSTRACT

Ultrawide bandgap (UWBG) semiconductors inherently exhibit very high electrical resistivities. This property presents not only challenges in probing their electrical transport properties but also difficulties to fabricate, understand, and characterize the electrical properties of metal contacts on these materials. Here, we report the measurements and analysis of the applied electric field dependence of photocurrent to reveal the effect of metal contacts on the transport properties of highly resistive h-BN. Our results indicate that even for h-BN with a room temperature resistivity as high as 10^{14} Ω cm, the as-deposited metal contact is not a completely blocking type as commonly assumed in previous analyses for other large bandgap insulating materials. By modifying the boundary condition between the metal/semiconductor interface, a quantitative description has been obtained, which can be used to determine if the metal contact is Ohmic or blocking type. This quantitative description should be applicable to all UWBG semiconductors with extremely high electrical resistivities. The work also provides a better understanding of how the metal contact type affects the transport properties of UWBG semiconductors in general.

While the group III-nitride wide bandgap (WBG) semiconductors have revolutionized the lighting, consumer electronics, and power electronics industries[1–9] and are making inroads in full spectrum solar energy conversion, sterilization, and UV curing device technologies,[10–12] ultrawide bandgap (UWBG) semiconductors have attracted increasing attention recently for applications in optics, photonics, and electronics beyond what have already been accomplished by WBG semiconductors.[13–15] One of the most difficult challenges in UWBG semiconductors is overcoming the issue of conductivity control. Not only limited to undoped UWBG semiconductors, acceptor-doped AlN, donor- and acceptor-doped BN, and donor-doped diamond often tend to exhibit poor electrical conductivities because of either deepening of the impurity energy level or more severe effect of deep-level impurity compensation on donor/acceptor doping with increasing energy bandgap.[13–28] The poor electrical conductivity control of UWBG semiconductors not only limits their potential applications but also poses difficulties in measuring and understanding the electrical transport properties of these materials. For example, the traditional Hall effect measurement technique, which has been employed as a standard method for monitoring the electrical transport properties of semiconductors, is difficult to perform at room temperatures on these UWBG semiconductors.[29] Another challenge confronting these highly resistive

semiconductors is the difficulty in preparing and analyzing the metal contacts for different applications. Metal contacts tend to end up with high contact resistances and high potential barriers between metal contacts and semiconductors. Moreover, a simple quantitative description for the understanding of properties of the metal contact and their effects on the carrier transport properties is still missing but is imperative for the advancement of UWBG semiconductor device technologies where both Ohmic and Schottky contacts are required.

While Hall effect measurements are difficult to perform on highly resistive UWBG semiconductors, photocurrents are relatively easy to measure because the dark currents tend to be very low in these materials. By measuring the applied electric field dependence of photocurrent, the charge carrier mobility-lifetime products, $\mu\tau$, can be obtained from a classical description developed by Many for large bandgap insulating materials.[30,31] This method has been used to guide the development of hexagonal BN (h-BN) quasi-bulk crystal growth and h-BN neutron detectors.[32–35]

The photocurrent density vs electric field (J-E) characteristics of highly resistive semiconducting materials have been extensively studied.[30–35] For the case of uniform carrier excitation throughout the crystal, the following classical equation was derived to describe the J-E characteristics, i.e., the relationship between the photocurrent density

(J) and applied electric field E by assuming that the metal contacts are perfectly blocking type for simplicity, i.e., Schottky contacts with an infinitely large barrier height,[30]

$$J(E) = J_o \frac{\mu\tau E}{W}\left[1 - \frac{\mu\tau E}{W}\left(1 - e^{-\frac{W}{\mu\tau E}}\right)\right]. \qquad (1)$$

In Eq. (1), $\mu\tau$ denotes the mobility-lifetime product of photogenerated charge carriers. W denotes the distance between the two metal contacts, E is the applied field (V/W), and J_0 is the saturation photocurrent density corresponding to $J(E)$ at $E \to \infty$, as can be extrapolated from the Taylor expansion of Eq. (1) with the condition of the drift length being much greater than the transit distance of the photogenerated carriers, $\mu\tau E \gg W$. More recently, Eq. (1) has been utilized to guide the development of h-BN quasi-bulk crystal growth by monitoring the $\mu\tau$ products.[32–35] However, it has been observed from time-to-time, the measured I-V (or J-E) characteristics of h-BN UWBG materials under photoexcitation deviate from Eq. (1),[32–35] the cause of which has not been understood.

Here, we report detailed experimental measurements and data analysis of the applied field dependence of photocurrent of h-BN. It was revealed that the type of metal contact plays a major role in the understanding of the photocurrent vs E behavior. While metal contacts deposited on these extremely high resistive UWBG semiconductors tend to be a blocking type as previously understood,[30,31] they are not 100% blocking contacts even for materials with extremely high resistivities, which corresponds more closely to practical situations. The applied field dependence of photocurrent is significantly influenced by many factors including the conditions of the metal contacts or metal–semiconductor interfaces. Here, we provide a quantitative description to aid understanding of metal contacts on these UWBG semiconductors. As achieving high quality contacts on UWBG semiconductors is one of the major obstacles in the field, finding an effective way to describe and understand the effects of metal contacts on UWBG semiconductors will be extremely valuable for the advancement of UWBG device technologies.

The thick ($\sim$100 μm in thickness) or quasi-bulk wafers of h-BN used in this study were produced by hydride vapor phase epitaxy (HVPE).[36–38] Natural boron trichloride (BCl_3) and NH_3 were used as precursors. The growth was conducted on c-plane sapphire of 2-in. in diameter. In contrast to metal organic chemical vapor deposition (MOCVD) growth technique, the HVPE method provides a faster

growth rate. Additionally, the precursors used in HVPE growth contain no carbon impurities.[36] Due to h-BN's layered structure, a thick h-BN wafer separates from the sapphire substrate after growth during the process of cooling down, from which a freestanding h-BN wafer was obtained.[32–38] The x-ray diffraction (XRD) spectra (θ–2θ scans) of these freestanding quasi-bulk crystals exhibit a dominant diffraction peak at 26.7°, corresponding to stacked planes in the c-direction and a c-lattice constant of 6.67 Å, associated with the hexagonal phase of BN.[36,37] Secondary ion mass spectrometry (SIMS) measurements revealed that the boron concentration is slightly less than the N concentration with a ratio of boron to nitrogen, [B]/[N] of 49.8/50.2.[37] The typical Raman spectra of these freestanding quasi-bulk crystals exhibit a mode at $\Delta\sigma = 1366$ cm^{-1}, corresponding to the E_{2g} vibration (in-plane stretch of B and N atoms) in bulk h-BN.[38]

For the electrical property characterization, as illustrated in Figs. 1(a)–1(c), lateral devices were fabricated from diced pieces of freestanding h-BN wafer to take advantage of the expected superior transport properties of h-BN with a layered crystalline structure.[33–36] Figure 1(a) shows a schematic diagram of a lateral device with metal contacts consisting of a bi-layer of Ni (100 nm)/Au (40 nm) deposited on its two edges using e-beam evaporation via a mask, which cover the entire vertical edges of the detector of 100 μm deep to ensure that the electric field is uniformly applied in the direction along the c-plane through the bulk of the detector material. Wire bonding was then performed to create electrical connections between the deposited metal contacts and the pads of a semiconductor device package. Figure 1(c) shows the photo of a device fabricated from a 100 μm thick wafer, with a width of W = 1.3 mm and a length of 10 mm. A laser driving light source (EQ99x LDLS) covering a wavelength range between 190 and 2400 nm was used as an excitation light source. A Kiethley sourcemeter was used to supply the bias voltage and an electrometer was used to record the photocurrent.

First, we conducted the dark electrical resistivity (ρ) measurements at room temperature. Figure 1(d) shows the dark I-V characteristics of h-BN, from which a room temperature dark resistivity of $\sim$1.4 $\times$ 10^{14} Ω cm is deduced. This value probably represents one of the highest resistivity values among all semiconductors studied thus far. A representative I-V (or J-E) characteristic under photoexcitation or the applied electrical field (E) dependence of photocurrent density (J) of h-BN is plotted in Fig. 2 (blue squares). The red curve in Fig. 2(a) is
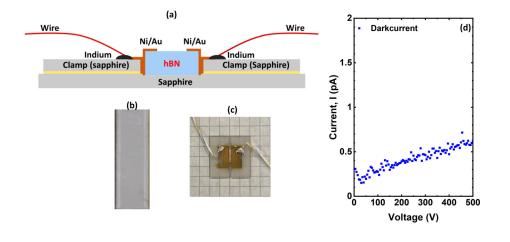

FIG. 1. (a) Schematic of a h-BN lateral device with metal contacts fabricated on the two edges, (b) photo of a diced h-BN strip for lateral detector fabrication, (c) a packaged lateral device used for photocurrent and contact studies, and (d) dark I-V characteristics of a fabricated h-BN lateral device.
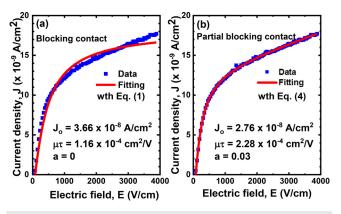
FIG. 2. (a) Measured applied electric field dependence of photocurrent density (blue solid dots) and least squares fitting (red curve) using Many's equation of Eq. (1). (b) Measured applied electric field dependence of photocurrent density (blue solid dots) and least squares fitting (red curve) using Eq. (4) with a modified boundary condition.

the least squares fitting of data with Eq. (1), which clearly reveals that the measured data deviate from the description of Eq. (1). More specifically, Eq. (1) predicts a saturation of photocurrent density under high electric fields, under the condition of $\mu\tau E \gg W$. However, the measured data clearly exhibit a linear increase in photocurrent density with E, at $E > 1.5 \times 10^3$ V/cm.

To understand the J-E characteristics under photoexcitation, let us review the conditions for obtaining Many's equation of Eq. (1). Equation (1) was derived with an assumption that metal contact to the highly resistive material is a perfect blocking type.[30] In the following, we will demonstrate how an amended Many's equation of photocurrent density vs E can be obtained by modifying the boundary condition between the metal contact and the highly resistive semiconductor, i.e., by changing the contact type from complete blocking to partial blocking or, more specifically, from Schottky contacts with an infinitely large barrier height to Schottky contacts with a finitely large barrier height.

Following the previous work for the case of uniform carrier excitation throughout the crystal,[30] the charge continuity condition gives

$$\mathcal{L} - \frac{p(z)}{\tau} - \mu E \frac{dp(z)}{dz} = 0, \qquad (2)$$

where $\mathcal{L}$ denotes the generation rate of photocarrier density, $p(z)$ denotes the charge carrier density at position z, τ denotes the charge carrier capture lifetime, and μ denotes the carrier mobility. The third term of Eq. (2) describes diffusion of photogenerated charge carriers, which are not uniformly distributed inside the semiconductors. Figure 3 (a) illustrates the scenario of a complete blocking metal contact, which gives rise to a boundary condition of $p(z = 0) = 0$, i.e., no charge carriers are injected from the negatively biased contact, and the photocurrent is due to photogenerated charge carriers inside the semiconductors. However, in practice, even in a semiconductor with an extremely high resistivity, the metal contact is not complete blocking type, instead it should be considered as a nearly perfect blocking, abiding a finite number of carries leaking from the negatively biased metal contact. The corresponding boundary condition must then be changed from $p(z = 0) = 0$ to $p(z = 0) = p_0$, as schematically illustrated in Fig. 3(b).

Solving Eq. (2) with a boundary condition of $p(z = 0) = p_0$ provides a solution of

$$p(z) = \mathcal{L}\tau\left[1 - (1 - a)e^{-\frac{z}{\mu\tau E}}\right], \qquad (3)$$

where $a = p_0/\mathcal{L}\tau$, which is a parameter describing the ratio of the charge carrier density at the boundary (interface between the negative biased metal contact and semiconductor) to the photogenerated carrier density inside the semiconductor. The electric field dependence of the photocurrent density is thus written as

$$J(E) = \frac{q\mu E}{W}\int_0^W p(z)dz = J_o\left(\frac{\mu\tau E}{W}\right)\left[1 - (1-a)\left(\frac{\mu\tau E}{W}\right)\left(1 - e^{-\frac{W}{\mu\tau E}}\right)\right],$$

$$(4)$$

where $J_0 = \mathcal{L}qW$. For $a = 0$ or $p_0 = 0$, Eq. (4) reduces to the original Many's solution of Eq. (1) as we expected. The case of $a \neq 0$ or $p_0 \neq 0$
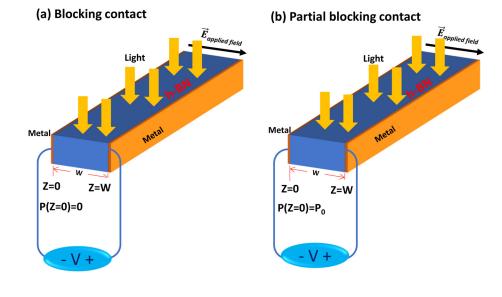
(a) Blocking contact   **(b) Partial blocking contact**

FIG. 3. Schematic illustrations of (a) a complete blocking metal contact with a boundary condition of $p_0 = p$ (z = 0) = 0 or $a = 0$ and (b) a partial blocking metal contact with a boundary condition of $p_0 \neq 0$ or $a \neq 0$.

corresponds to a partial blocking contact. Therefore, parameter a is a measure of percentage of Ohmic vs blocking contact type, to be discussed in more detail below.

Figure 2(b) shows the least squares fitting of the measured data with Eq. (4), demonstrating a perfect agreement with the fitted value of $a = 0.03$. The results indicate that the metal contact is almost of perfect blocking type (97%) but with a small fraction (3%) of charge carriers "leaking" through the negatively biased metal contact. The behavior of the linear increase in photocurrent with E at higher fields can be understood by the following analysis. At low fields with $\mu\tau E/W < 1$, Eq. (4) reduces to

$$J_{\text{small-E}} = (\mathcal{L}\tau)q\mu E = \sigma_{\text{small-E}}\,E, \qquad (5)$$

where $\sigma_{\text{small-E}}$ denotes the effective electrical conductivity in the low field region with a photogenerated charge carrier density of $(\mathcal{L}\tau)$. At higher fields with $\mu\tau E/W \gg 1$, Eq. (4) reduces to

$$J_{\text{large-E}} = J_0(1-a)/2 + a\mathcal{L}\,q\mu\tau E = J_0(1-a)/2 + \sigma_{\text{large-E}}\,E$$
$$= J_0(1-a)/2 + a\sigma_{\text{small-E}}\,E. \qquad (6)$$

Here, $\sigma_{\text{large-E}}$ denotes the effective electrical conductivity at higher fields with a photogenerated charge carrier density of $(\mathcal{L}\tau)$. From Eq. (6), we have $\sigma_{\text{large-E}} = a\sigma_{\text{small-E}}$. Now, returning to the cause of the linear increase in J with E under higher fields, it becomes clear that this behavior is due to carriers leaking through this nearly perfect blocking metal contact. The linear increase in photocurrent at higher fields is related to the initial linear increase in photocurrent with E through this value of a.

To provide a better understanding of parameter a, we measured the J-E characteristics under different excitation powers (P) for (a) P = 0.2 mW, (b) P = 0.1 mW, and (c) P = 0.06 mW, and the results are plotted in Fig. 4. The solid dots are the measured data, and the red curves are fittings with Eq. (4), exhibiting perfect agreements for all three values of P. The slopes of the linear plots in the large and small field regions provide values of $\sigma_{\text{large-E}}$ and $\sigma_{\text{small-E}}$, respectively, indicated as blue solid and dotted lines.

The fitting results shown in Fig. 4 are summarized in Fig. 5, showing the excitation power (P) dependencies of the measured parameters of (a) $\mu\tau$, (b) J_0, and (c) parameter a. The mobility-lifetime product $\mu\tau$ decreases with an increase in P. Since carrier mobility (μ)
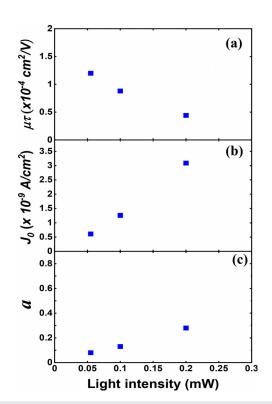
FIG. 5. Excitation power (P) dependencies of measured parameters in J-E characteristics of (a) carrier mobility-lifetime product $\mu\tau$, (b) saturation current density J_0, and (c) parameter a.

is not expected to be changed significantly with photogenerated carrier density, the results in Fig. 5(a) thus suggest that the carrier capture lifetime decreases with an increase in P. The results of Fig. 5(b) indicate that J_0 increases linearly with an increase in P, which is expected since J_0 is related to the generation rate of photocarrier density $(\mathcal{L})$, which increases linearly with P. Figure 5(c) shows that parameter a increases with an increase in P, which means that the photogenerated charge carrier density at boundary $z = 0$ (p_0) increases with P, since $p_0 = a\mathcal{L}\tau$. This dependence of parameter a on P is also expected from our
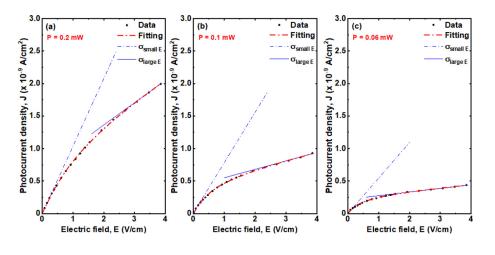
FIG. 4. Applied electric field (E) dependence of photocurrent density measured at three different excitation powers of (a) P = 0.2 mW, (b) P = 0.1 mW, and (c) P = 0.06 mW. The solid dots are the measured data, and the red curves are the least squares fitting with Eq. (4). The behaviors of the linear increase in photocurrent density with E in the small and large electric field regions are also indicated with dotted and solid blue lines, respectively.

TABLE I. Parameters of the J-E characteristics measured under different excitation powers obtained by fitting the measured data with Eq. (4) as shown in Fig. 4.

Parameter $\qquad$ P (mW)	0.06	0.1	0.2
$J_o \left(10^{-9}\,\text{A/cm}^2\right)$	0.61	1.26	3.09
$\mu\tau \left(10^{-4}\,\text{cm}^2/\text{V}\right)$	1.2	0.88	0.44
$\mathcal{L} \left(10^{11}/\text{cm}^3\,\text{s}\right)$	0.29	0.61	1.48
$\sigma_{small\,E} \left(10^{-13}/\Omega\,\text{cm}\right)$	5.48	9.30	12.3
$\sigma_{large\,E} \left(10^{-13}/\Omega\,\text{cm}\right)$	0.56	1.3	3.4
$a = \dfrac{\sigma_{large-E}}{\sigma_{small-E}}$	0.10	0.14	0.28
a [fitted by Eq. (4)]	0.08	0.13	0.28

discussion. As the excitation power (P) increases, more charge carriers are generated inside the semiconductor and consequently the electrical conductivity of semiconductor enhances, making the metal contact less blocking but more Ohmic type. This is equivalently saying that metal contacts become less perfect blocking but more Ohmic with increasing a.

Table I lists the parameters of the J-E characteristics measured under different excitation powers obtained from Figs. 4 and 5. The values of a can be obtained either directly from fitting the measured J vs E curves with Eq. (4) or from the ratio of $\sigma_{lage\text{-}E}$ to $\sigma_{small\text{-}E}$. The derived values of a from $a = \sigma_{large\text{-}E}/\sigma_{small\text{-}E}$ agree very well with those obtained from fitting between the measured J vs E characteristics and Eq. (4) for all three excitation power values. These results validate our analysis.

It is important to emphasize that the linear increase in the photo-current density with increasing E observed at large E values is because the metal contact is not completely the blocking type, which is expected from practical situations. In most practical instances, the value of a can be very small but not zero even for very high resistive materials. The metal contact is a partial blocking and partial Ohmic type if $0 < a < 1$. It is a complete blocking contact if $a = 0$, reducing to the case described by Eq. (1).[30] The contact is an Ohmic type if $a = 1$, resulting in a linear increase in photocurrent density with applied field (E) for all values of E, following the description of Eq. (4). Realizing a large value of a, meaning metal contact is predominantly Ohmic type, is highly desirable for many device applications, but is not easy to achieve for highly resistive UWBG semiconductors. The small values of a (near 0) implies that the metal contact is predominantly blocking type and accompanied with only slight Ohmic behavior, as the cases investigated here. This is consistent with our expectation since h-BN investigated here has a resistivity as high as $10^{14}\,\Omega\,\text{cm}$. However, this partial Ohmic behavior is critical to account for the observed electric field dependence of photocurrent density at high fields. If we examine the metal contacts from the conductivity point of view, parameter a increases with excitation power (P) as shown in Fig. 5(c). This implies that the metal contact type evolves toward Ohmic from blocking as the materials' electrical conductivity increases, which is consistent with our expectation. The most important implication of our results is that we have in our disposal a quantitative and effective way to monitor the type of metal contact on very high resistive UWBG semiconductors.

In summary, a quantitative description for metal contact on highly resistive UWBG materials has been obtained by investigating the applied field dependence of photocurrent of highly resistive h-BN. Our results indicate that even for highly resistive materials such as h-BN with an electrical resistivity as high as $10^{14}\,\Omega\,\text{cm}$ studied here, metal contacts are not a completely blocking type as widely assumed in earlier works. By modifying the boundary condition between the metal/semiconductor interface, a quantitative description has been obtained, which can be used to determine quantitively the degree of metal contacts being Ohmic or blocking type. This quantitative description is expressed by parameter a, which describes the ratio of the carrier density at the boundary of negatively biased metal contact to the charge carrier density inside the semiconductor. The case of $a = 0$ corresponds to a perfect blocking contact, while a non-zero but small value a indicates a partial Ohmic characteristic with charge carriers leaking through the negatively biased metal contact. Though the experimental results and analysis reported here are obtained from h-BN, the same analysis should be applicable to all highly resistive UWBG semiconductors. It is widely recognized that realizing high quality contacts on UBWG semiconductors remains one of the foremost challenges. The results presented here will help to guide the preparation of improved metal contacts on UBWG semiconductors for different applications as well as for the understanding of the electrical and photonic properties of UBWG semiconductors.

AUTHOR DECLARATIONS
Conflict of Interest

The authors have no conflicts to disclose.

Author Contributions

A. Tingsuwatit: Data curation (equal); Formal analysis (equal); Investigation (equal); Methodology (equal); Software (equal); Validation (equal); Visualization (equal). **N. K. Hossain:** Data curation (equal); Formal analysis (equal); Investigation (equal); Methodology (equal); Software (equal); Validation (equal); Visualization (equal). **Z. Alemoush:** Data curation (equal); Formal analysis (equal); Investigation (equal); Methodology (equal); Software (equal); Validation (equal); Visualization (equal). **M. Almohammad:** Data curation (equal); Formal analysis (equal); Investigation (equal); Methodology (equal); Project administration (equal); Resources (equal); Software (equal); Supervision (equal); Validation (equal); Visualization (equal). **J. Li:** Conceptualization (equal); Data curation (equal); Formal analysis (equal); Funding acquisition (equal); Investigation (equal); Methodology (equal); Project administration (equal); Resources (equal); Software (equal); Supervision (equal); Validation (equal); Visualization (equal); Writing – original draft (equal); Writing – review & editing (equal). **J. Y. Lin:** Conceptualization (equal); Formal analysis (equal); Funding acquisition (equal); Investigation (equal); Methodology (equal); Project administration (equal); Resources (equal); Supervision (equal); Validation (equal); Visualization (equal); Writing – original draft (equal); Writing – review & editing (equal). **H. X. Jiang:** Conceptualization (equal); Data curation (equal); Formal analysis (equal); Funding acquisition (equal);

Investigation (equal); Methodology (equal); Project administration (equal); Resources (equal); Software (equal); Supervision (equal); Validation (equal); Visualization (equal); Writing – original draft (equal); Writing – review & editing (equal).

DATA AVAILABILITY

The data that support the findings of this study are available within the article.

REFERENCES

[1] See https://www.nobelprize.org/prizes/physics/2014/press-release/ for "New light to illuminate the world" (2014).

[2] S. Nakamura, S. J. Pearton, and G. Fasol, *The Blue Laser Diode* (Springer, Berlin, Heidelberg, 2000).

[3] H. Amano, N. Sawaki, I. Akasaki, and Y. Toyoda, Appl. Phys. Lett. **48**, 353 (1986).

[4] S. Nakamura, T. Mukai, and M. Senoh, Appl. Phys. Lett. **64**, 1687 (1994).

[5] T. D. Moustakas, U.S. Patent No. 5,686,738 (11 November 1997).

[6] H. X. Jiang and J. Y. Lin, Nat. Electron. **6**, 257 (2023).

[7] P. J. Parbrook, B. Corbett, J. Han, T. Y. Seong, and H. Amano, Laser Photonics Rev. **15**, 2000133 (2021).

[8] H. Amano, Y. Baines, E. Beam *et al.*, J. Phys. D: Appl. Phys. **51**, 163001 (2018).

[9] I. C. Kizilyalli, O. B. Spahn, and E. P. Carlson, ECS Trans. **109**, 3 (2022).

[10] J. Wu, W. Walukiewicz, K. Yu, J. W. Ager III, E. E. Haller, H. Lu, W. J. Schaff, Y. Saito, and Y. Nanishi, Appl. Phys. Lett. **80**, 4741 (2002).

[11] S. Vanka, B. Zhou, R. A. Awni, Z. Song, F. A. Chowdhury, X. Liu, H. Hajibabaei, W. Shi, Y. Xiao, I. A. Navid, A. Pandey, R. Chen, G. A. Botton, T. W. Hamann, D. Wang, Y. Yan, and Z. Mi, ACS Energy Lett. **5**, 3741 (2020).

[12] B. C. Letson, S. Barke, S. P. Kenyon, T. Olatunde, G. Mueller, P. Wass, F. Ren, S. J. Pearton, and J. W. Conklin, Rev. Sci. Instrum. **93**, 114503 (2022).

[13] "Ultrawide bandgap semiconductors," in *Semiconductors and Semimetals*, edited by Y. Zhao and Z. Mi (Academic Press, an imprint of Elsevier, 2021), Vol. 107.

[14] M. Higashiwaki, R. Kaplar, J. Pernot, and H. Zhao, Appl. Phys. Lett. **118**, 200401 (2021).

[15] J. Y. Tsao, S. Chowdhury, M. A. Hollis, D. Jena *et al.*, Adv. Electron. Mater. **4**, 1600501 (2018).

[16] K. B. Nam, M. L. Nakarmi, J. Li, J. Y. Lin, and H. X. Jiang, Appl. Phys. Lett. **83**, 878 (2003).

[17] C. G. V. de Walle and J. Neugebauer, J. Appl. Phys. **95**, 3851 (2004).

[18] Y. Taniyasu, M. Kasu, and T. Makimoto, Nature **441**, 325 (2006).

[19] F. Mehnke, X. Thang, T. Harald Pinge, T. Wernicke1, E. Janzén, N. T. Son, and M. Kneissl, J. Appl. Phys. **120**, 145702 (2016).

[20] I. Bryan, Z. Bryan, S. Washiyama, P. Reddy, B. Gaddy, B. Sarkar, M. Hayden Breckenridge, Q. Guo, M. Bobea, J. Tweedie, S. Mita, D. Irving, R. Collazo, and Z. Sitar, Appl. Phys. Lett. **112**, 062102 (2018).

[21] H. Ahmad, Z. Engel, C. M. Matthews, S. Lee, and W. A. Doolittle, J. Appl. Phys. **131**, 175701 (2022).

[22] F. Oba, A. Togo, I. Tanaka, K. Watanabe, and T. Taniguchi, Phys. Rev. B **81**, 075125 (2010).

[23] L. Weston, D. Wickramaratne, M. Mackoit, A. Alkauskas, and C. G. Van de Walle, Phys. Rev. B **97**, 214104 (2018).

[24] B. He, W. J. Zhang, Z. Q. Yao, Y. M. Chong, Y. Yang, Q. Ye, X. J. Pan, J. A. Zapien, I. Bello, S. T. Lee, I. Gerhards, H. Zutz, and H. Hofsäss, Appl. Phys. Lett. **95**, 252106 (2009).

[25] W. J. Zhang, Y. M. Chong, I. Bello, and S. T. Lee, J. Phys. D: Appl. Phys. **40**, 6159 (2007).

[26] T. Joshi, P. Kumar, B. Poudyal, S. P. Russell, P. Manchanda, and P. Dev, Phys. Rev. B **105**, 054101 (2022).

[27] S. Koizumi, K. Watanabe, M. Hasegawa, and H. Kanda, Science **292**, 1899 (2001).

[28] M. A. Pinault, J. Barjon, T. Kociniewski, F. Jomard, and J. Chevallier, Physica B **401-402**, 51 (2007).

[29] S. Majety, T. C. Doan, J. Li, J. Y. Lin, and H. X. Jiang, AIP Adv. **3**, 122116 (2013).

[30] A. Many, J. Phys. Chem. Solids **26**, 575 (1965).

[31] U. Lachish, Nucl. Instrum. Methods Phys. Res. A **403**, 417 (1998).

[32] A. Maity, T. C. Doan, J. Li, J. Y. Lin, and H. X. Jiang, Appl. Phys. Lett. **109**, 072101 (2016).

[33] A. Maity, S. J. Grenadier, J. Li, J. Y. Lin, and H. X. Jiang, Appl. Phys. Lett. **116**, 142102 (2020).

[34] A. Maity, S. J. Grenadier, J. Li, J. Y. Lin, and H. X. Jiang, Prog. Quantum. Electron. **76**, 100302 (2021).

[35] S. J. Grenadier, A. Maity, J. Li, J. Y. Lin, and H. X. Jiang, "Electrical transport properties of hexagonal boron nitride epilayers," in *Semiconductors and Semimetals*, Ultrawide Bandgap Semiconductors, edited by Y. Zhao and Z. Mi (Elsevier, Amsterdam, 2021), Vol. 107, p. 393.

[36] Z. Alemoush, N. K. Hossain, A. Tingsuwatit, M. Almohammad, J. Li, J. Y. Lin, and H. X. Jiang, Appl. Phys. Lett. **122**, 012105 (2023).

[37] Z. Alemoush, A. Tingsuwatit, J. Li, J. Y. Lin, and H. X. Jiang, Crystals **13**, 1319 (2023).

[38] M. Almohammad, Z. Alemoush, J. Li, J. Y. Lin, and H. X. Jiang, Appl. Phys. Lett. **124**, 102106 (2024).

18 April 2024 20:01:51